Object Detection Using High-Resolution Near-Field Array Processing*

Adnan Şahin and Eric L. Miller
Center for Electromagnetics Research,
235 Forsyth Building, 360 Huntington Ave.
Northeastern University, Boston, MA 02115
Telephone: (617) 373-8386
Telefax : (617) 373-8627
email: adnan@cdsp.neu.edu

April 24, 1998

Abstract

In this paper we present an algorithm for the detection and localization of an unknown number of objects present in the near field of a linear receiver array. To overcome the nonplanar nature of the wavefield over the array, the full array is divided into a collection of sub-arrays, such that the scattered fields from objects are locally planar at each sub-array. Using the MUSIC algorithm, directions of arrival (DOA) of locally planar waves at each sub-array are found. By triangulating these DOAs, a set of crossings, condensed around expected object locations, are obtained. To process this spatial crossing pattern, we develop a statistical model for the distribution of these crossings and employ hypothesis testing techniques to identify a collection of small windows likely to contain targets. Finally, the results of the hypothesis tests are used to estimate the number and locations of the targets. Using simulated data, we demonstrate usefulness and performance of this approach for typical background electrical properties and signal to noise ratios.

*This work was supported by the Department of Energy under contract DE-FC07-95ID13395, the Army Research Office Demining MURI under Grant DAAG55-97-1-0013, an ODDR&E MURI under Air Force Office of Scientific Research contract F49620-96-1-0028, and a CAREER Award from the National Science Foundation MIP-9623721

1 Introduction

The problem of detection and localization of objects in the near field of an antenna array has arisen in a number of application areas in recent years. For example, in the area of landmine remediation, the goal is to find relatively small, metallic and plastic objects located in a lossy medium (the soil) but a few centimeters from the transmitters and receivers. Alternatively, for purposes of environmental remediation, the targets of interest tend to be larger (eg. steel metal drums filled with hazardous waste), and located on the order of meters from the array. Although several near-field array processing methods have been reported in the literature, their use has been restricted to the localization of independent sources radiating spherical waves [1–3] and are thus not suited to the problem of interest in this work: the detection and localization of extended targets illuminated by an incident plane wave and positioned such that multiple scattering effects cannot be ignored.

The problem of target detection and localization for these and related applications often is addressed by using the data to produce a pixel-by-pixel map of the region near the array and then post-processing the image to localize the objects [4–8]. Since the initial image generation represents an ill-posed inverse problem, a stable solution requires the use of a regularization method [9]. Unfortunately, typical regularizers result in smooth images thereby making the detection all the more difficult. In this paper, we develop an alternate approach to target detection and localization which bypasses this difficult step of image generation and is aimed at extracting the number of objects and their locations more directly from the data.

Of particular interest is the measurement geometry shown in Fig. 1. A plane wave illuminates the region of interest assumed to be a homogeneous, possibly lossy medium containing one or more targets located in the near field of an array of receivers. The inherent array structure of

the measurement geometry suggests that the high resolution array processing techniques [10,11] quite popular in the signal processing community would be well suited for the near-field detection problem. Adapting such methods to the problem of interest here presents a collection of interesting challenges. First, these array processing techniques typically assume that the sources are infinitely far away so that the waveform received on the array is planar. For our problem, since the objects are located relatively close to the receiver array, this key assumption is not valid. Second, for such near-field objects both range as well as the direction of arrival has to be determined in order to localize the object. Finally, a problem common to both the near-field and far-field array processing algorithms is that the number of incident waveforms/targets is not known *a priori*.

To deal with the nonplanar nature of the wavefronts over the array, we partition the receiver array into sub-arrays, such that the scattered field is locally planar at each sub-array. Then, using high resolution array processing techniques, each sub-array identifies a single direction of arrival (DOA) corresponding to the most dominant scatterer in the vicinity of that sub-array. The localization of the objects in terms of their ranges and bearings is achieved by triangulating the directions of arrival from all subarrays which in turn results in a crossing pattern of DOA intersections. Examination of typical crossing structures reveals that there are two distinct patterns where the crossings are either dense or sparse. Dense crossing regions clearly indicate object locations and are distinguished from "background" regions where the crossings are sparse. The problem of object detection and localization then is reduced to the processing of the crossings obtained from our triangulation procedure.

For this purpose, we introduce a simple yet accurate stochastic model describing the spatial distribution of DOA crossings. Such modeling is warranted for two reasons. First, due to the noise in the data, the DOA intersection points are inherently randomly distributed in the plane. Second,

such modeling forms a solid basis for algorithm development and quantitative performance analysis in the form of detection and false alarm rates.

In this work, we model the two classes of crossings (dense vs. sparse) using a pair of spatial Poisson distributions [12]. The Poisson model in the target region has a large rate parameter while that of the background region is considerably smaller. Based on these target and background models, we develop a hypothesis testing technique for the joint estimation of the rate parameters and the localization of dense crossing regions which indicate the existence of targets. Simple post-processing of the hypothesis testing results provides both the number of targets and estimates of their locations. Finally, we verify that the a Poisson model is in fact a rather accurate description of the spatial distribution of crossings.

We demonstrate the performance of this approach for the detection and localization of multiple mine-like and drum-like targets located in the near field of the receiver array. For mine-like targets relative positions of the objects are changed to see the effect of object geometry on detectability. We show that the detectability improves, and false alarm rate decreases as the objects are located far apart. For drum-like targets, we demonstrate the effect of relative depth as well as relative distance between objects on detectability.

The remainder of this paper is organized as follows. In Section 2 we describe the models and notation used in the paper, in Section 3 we introduce the detection algorithm and hypothesis testing. Examples depicting performance of the algorithm are given in Section 4 and in Section 5 we will draw conclusions and suggest future work.

2 Background

The multi, bi-static measurement scheme depicted in Fig. 1 is considered in this paper. A perpendicularly polarized plane wave, $E_i(\mathbf{r})$, impinges on a collection of objects in a known background, inducing surface and volume currents which in turn radiate a scattered field, $E_s(\mathbf{r})$[1]. The scattered electric field from the targets is spatially sampled by a uniformly spaced, N-element linear array with isotropic receiver characteristics. The measured data at the sensor outputs are:

$$\mathbf{x} = \mathbf{E_s} + \mathbf{n}, \tag{1}$$

where $\mathbf{E_s} = [E_s(\mathbf{r_1})\ \ E_s(\mathbf{r_2}) \cdots E_s(\mathbf{r_N})]^T$, $\mathbf{r_i}$ is the vector from the origin to the ith receiver location and $\mathbf{n}$ is zero mean, white Gaussian noise.

The structure of the receivers in Fig. 1 coupled with the underlying problem of target detection suggests the use of array processing methods for localizing buried targets. In this paper we consider the MUSIC (Multiple Signal Classification) [13] algorithm. Traditionally, MUSIC and other direction finding techniques are used to determine directions of arrival (DOA) of plane waves to a receiver array. Here, we adapt MUSIC to the near-field detection problem.

To make use of the MUSIC algorithm, the experiment as represented by (1) is repeated many times to determine the statistics of $\mathbf{x}$. In particular, if L scattering experiments are performed, then the maximum likelihood estimate of the spatial autocovariance matrix $\mathbf{R}$ is given by [10]:

$$\hat{\mathbf{R}} = \frac{1}{L}\sum_{l=1}^{L} \mathbf{x}_l \mathbf{x}_l^H \tag{2}$$

where $\mathbf{x}_l$ is the data measured at the lth experiment, and superscript H denotes conjugate transpose. Then, the eigenspace decomposition of $\hat{\mathbf{R}}$ yields [10]:

$$\hat{\mathbf{R}} = \hat{\mathbf{U}}_s \hat{\mathbf{\Lambda}}_s \hat{\mathbf{U}}_s^H + \hat{\mathbf{U}}_n [\hat{\sigma}^2 \mathbf{I}] \hat{\mathbf{U}}_n^H \tag{3}$$

where $\hat{\mathbf{U}}_s$ is the estimated signal subspace matrix and contains the M signal eigenvectors, and $\hat{\mathbf{U}}_n$

[1] All analysis is in frequency domain, thus the $e^{j\omega t}$ dependence is suppressed

is the estimated noise subspace matrix and contains $N - M$ noise eigenvectors of multiple noise eigenvalue $\hat{\sigma}^2$. The projection operator onto the noise subspace is defined as [10]:

$$\hat{\mathbf{\Pi}}_{\mathbf{n}} = \hat{\mathbf{U}}_n \hat{\mathbf{U}}_n^H. \tag{4}$$

Assuming plane wave incidence on the array, the idea behind MUSIC is that the reciprocal of the "distance" between the estimated noise subspace and the true noise subspace has sharp peaks around the DOAs. Thus, if one plots this quantity versus all possible angles, estimates of DOAs can be determined by the maxima of the resulting angular spectrum which is given by [10]:

$$P_{MUSIC}(\theta) = \frac{\mathbf{a}(\theta)^H \mathbf{a}(\theta)}{\mathbf{a}(\theta)^H \hat{\mathbf{\Pi}}_n \mathbf{a}(\theta)} \tag{5}$$

where $\mathbf{a}(\theta) = [1 \quad e^{j\beta d\cos\theta} \quad e^{j2\beta d\cos\theta} \ldots e^{j(N-1)\beta d\cos\theta}]^T$ is the direction vector, β is the wave number in the medium of propagation, and d is the distance between two receivers.

As stated previously this formulation of the array processing problem assumes that the radiator is infinitely distant so that the scattered field has planar wavefronts and the elements of the direction vector $\mathbf{a}(\theta)$ are complex exponentials. However for the problems of interest here, the receivers are in the near-field region of the radiating sources, resulting in non-planar wavefronts. Additionally, the target localization problem not only requires the DOA relative to the array but also the range of the target from a point on the array (eg. the leftmost element.)

3 Algorithm

A key element of the work in this paper is the development of a sub-array processing method for detection of multiple objects in the near field of an array. In a previous work [14], we have examined such a technique for detection and localization of single metallic and dielectric objects. As illustrated in Fig. 2 (and as is generally the case), the localization problem in [14] is straightforward since typically all crossings are densely packed within the radius of the object. Therefore, the location of the object can be inferred quite easily. For multiple objects, however, the crossing pattern is

quite complicated, since DOAs of different objects create unwanted crossings as shown in Fig. 3. The clusters of object crossings are embedded in this unwanted background crossings, and have to be extracted carefully. Thus, in this work, we concentrate exclusively on the problem of multiple object detection.

Before introducing the details of our approach, we want to briefly describe the algorithm with the help of flow chart in Fig. 4. The algorithm proceeds as follows:

1. **Sub-array processing:** At this stage of the algorithm, we partition the receiver array so that the observed scattered field is locally planar at each sub-array. The directions of arrival (DOAs) are found using MUSIC as if planar waves are impinging on the sub-arrays. The DOAs are then triangulated to obtain the crossing pattern. This stage of the algorithm is repeated several times for plane waves at different temporal frequencies to improve performance and resolution. The crossing patterns obtained at different frequencies are overlaid to yield an aggregate crossing pattern which is, then, passed onto the second stage of the algorithm.

2. **Crossing analysis:** In the second stage, the crossing pattern is modeled with two Poisson counting processes, corresponding to target and background regions. After estimating the required rate parameters using the crossing data, a hypothesis testing procedure is employed to determine a set of "window" regions corresponding to areas containing targets.

3. **Target extraction:** At the final stage of the algorithm, the individual detection windows are aggregated into a number of spatially disjoint groups. The total number of groups indicates the estimated number of targets, and average coordinates of all windows in a group indicate the estimated center of the corresponding target.

3.1 Sub-array Processing

The direction finding algorithms traditionally assume plane wave incidences and determine the DOA associated with each plane wave. For near-field problems, however, both DOA and the range of the source (in our case scatterer) should be acquired. Here, we describe a sub-array processing (SAP) scheme which only requires one-dimensional search in DOA space of each sub-array. The idea behind the sub-array processing is that if the aperture of the sub-array is small enough, the scattered field impinging upon it can be assumed locally planar. Thus, the plane wave MUSIC can be used to find DOAs at each sub-array, and by triangulation, it is possible to localize the scatterers.

When there are $M > 1$ objects in the vicinity of the array, we have two options in terms of how MUSIC is employed:

1. Each sub-array finds M DOAs for all locally planar waves scattered from M objects, or

2. Each sub-array finds one DOA for the locally planar wave dominant in the total scattered field (Fig. 3 shows $M = 2$ case).

Given M objects and S sub-arrays, for each operating frequency the first and second options result in $0.5SM(SM-1)$ and $0.5S(S-1)$ crossings, respectively. The first option creates many unwanted crossings when DOAs belonging to different objects intersect. In addition, we have to know the number of objects under the array to use this option. On the other hand, the second option does not require the knowledge of number of objects, and the scattered fields from targets closer to the sub-arrays, particularly in a lossy medium such as soil, dominate the total scattered field at the sub-arrays. Therefore, the latter option seems more practical especially when one wants to avoid estimating the number of scatterers first, and is used in the remainder of this paper.

Once one DOA at each sub-array is determined, all DOAs are triangulated to estimate the target locations. Fig. 3(a) shows the triangulation of DOAs, and (b) shows the crossings. In contrast to the single object case, for multiple objects, the crossing pattern may get quite complicated since DOAs belonging to different objects also intersect each other to create unwanted crossings. Thus, a second level of processing is required to extract the clusters indicating the estimated object centers.

3.2 Crossing Analysis

In this section we present an approach that models the DOA crossings with Poisson point processes. Inspecting Fig. 3(b), we see two distinct regions where the density of the crossings are quite different: in the first region (*background region*) the crossings are sparse, and in the second region (*target region*) the crossings are dense. By exploiting this difference, it is possible to isolate target locations. Hence, we introduce a Poisson model for DOA crossings which has a large rate parameter (intensity) in target regions and a small rate parameter in the background region.

Formally, for a given crossing pattern, we count the number of crossing Y_j, $j = 1, 2, \cdots, N_y$, in a window of size $w_x \times w_y$, where N_y is the total number of *non-overlapping* windows, w_x and w_y are the width of the windows in x and y directions, respectively. The windows must be non-overlapping to guarantee the independence of random variables Y_j.

In order to ensure that Y_j is Poisson distributed, we tested for fitness to Poisson distribution by using the graphical technique presented in [15]. The technique proposes that for each count k observed in Y_j, we plot k versus $(\ln k! + \ln F_k)$ where $F_k = \sum_{j=1}^{N_y} [Y_j = k]$ is the number of data values Y_j equal to k. If the fit to the Poisson model is satisfactory, then the plot should form a straight line with slope approximately $\ln \lambda$, where λ is the rate parameter of the distribution. When we apply this test to a typical crossing pattern, instead of a straight line, we observed the curve in Fig. 5. By examining this curve, we notice that it can be decomposed into two parts, each roughly

corresponding to a straight line. The first part is when the crossing count k is small (between 0 and 2), and the second part is when k is large (greater than 3.) It is clear that these two regions correspond to the background process which is expected to have a small count of crossings, and the target process which is expected to have a large count of crossings. Furthermore, using these two approximately linear regions, we can decouple background and target processes by identifying k_b and F_{kb} for the background, and k_t and F_{kt} for the target regions where $k_b = 0, 1, 2$, $k_t = 3, 4, \cdots$, $F_{kb} = \sum_{j=1}^{N_y} [Y_j = k_b]$ and $F_{kt} = \sum_{j=1}^{N_y} [Y_j = k_t]$. Then, the rate parameters for the background and the target regions are given by their maximum likelihood estimators [15]:

$$\hat{\lambda}_b = \frac{1}{N_b} \sum_{kb=0}^{2} k_b F_{kb}, \tag{6}$$

and

$$\hat{\lambda}_t = \frac{1}{N_t} \sum_{k_t=3}^{\infty} k_t F_{kt}, \tag{7}$$

where $N_b = \sum_{k_b} F_{kb}$ and $N_t = \sum_{k_t} F_{kt}$. Having estimated $\hat{\lambda}_b$ and $\hat{\lambda}_t$, the probability mass functions in the background and target regions can be expressed as:

$$f_X(k|\text{Background}) = P\{X = k|\text{Background}\} = \frac{1}{k!} e^{-\hat{\lambda}_b} \hat{\lambda}_b^k \tag{8}$$

and

$$f_X(k|\text{Target}) = P\{X = k|\text{Target}\} = \frac{1}{k!} e^{-\hat{\lambda}_b} \hat{\lambda}_b^k. \tag{9}$$

To extract crossing clusters, we sweep the region of interest with a test window of size $w_x \times w_y$. It is important that the area of the test window is equal to the area of the non-overlapping windows used in estimating the rate parameters. At each location of the test window, we count the number of crossings T_j, $j = 1, 2, \cdots, N_{test}$, where N_{test} is the total number of *overlapping* sweep windows in the region of interest. The number of overlapping test windows N_{test} defines the resolution of detection, and it is greater than N_y. Since we are going to test each T_j against the hypothesis one by one, the use of overlapping windows is allowed. Hypothesis test permits us determine whether

the test window is over a background region or over a target region. The hypothesis test is then formally written as:

- H_0: T_j is Poisson distributed with a small rate parameter $\hat{\lambda}_b$,
- H_1: T_j is Poisson distributed with a large rate parameter $\hat{\lambda}_t$.

Based on this hypothesis test, if H_0 is true, we decide that the window belongs to a background process with a small intensity. However, if H_1 is true, we declare that the window belongs to a target process with a large intensity and call it a detection.

The likelihood ratio for the hypothesis test is formed in terms of the probability mass functions of (8) and (9) as:

$$\Lambda(T_j) = \frac{f_X(T_j|H_1)}{f_X(T_j|H_0)}$$

The decision is, then, made based on the test:

$$\ln\{\Lambda(T_j)\} = T_j \overset{H_1}{>} K,$$

where the decision threshold, K, is found from a specified false alarm rate P_{fa} using (10). This means that all windows which has K or more crossings in them will be declared as target locations. Probability of false alarm P_{fa} can be written in terms of the decision threshold K and probability mass function of background process in (8) as :

$$P_{fa} = \sum_{k=K}^{\infty} f_X(k|H_0). \tag{10}$$

Given the decision threshold K, the probability of detection for the Poisson model developed in this section is given by:

$$P_d = \sum_{k=K}^{\infty} f_X(k|H_1). \tag{11}$$

It might be argued that since target windows are obtained via thresholding, there would be no need for a Poisson-based model as described in this section. A plain thresholding scheme on DOA

crossings would also locate the targets successfully. However, the Poisson model provides a solid groundwork for a detailed statistical analysis. With the model, it is possible to define probabilities of false alarm and detection. Based on these statistical analyses, it is possible to make educated predictions about the performance of the system under different conditions.

3.3 Target Extraction

Hypothesis testing with the Poisson model results in detection windows as shown in Fig. 6. By looking at this figure, a human operator may conclude the target locations and their numbers. However, we want the detection algorithm to do these decisions and calculations for us automatically. In effect, we want the algorithm to yield the number of targets in the region of interest and their estimated locations, rather than the intertwined pattern of detection windows.

The pattern of detection windows suggests that the detection windows belonging to the same targets overlap. Therefore, we classify the detection windows so that all overlapping windows form a different group. The number of targets is, then, equal to the number of groups and the estimated object centers are obtained by averaging the coordinates of the windows in each group. The grouping algorithm we use, therefore, proceeds as follows. Start with the first window on the list of detection windows and place it in the first group. For each of the other windows, test if they overlap with any window in the kth group for $k = 1, 2, \cdots, G_c$, where G_c is the number of currently available groups. If the window overlaps with only one group, add it to that group. If the window overlaps with more than one groups, merge those groups, and reduce the number of current groups G_c accordingly. If the window does not overlap with any windows among G_c groups, then form (G_c+1)th group with that window. When all detection windows are classified, G_c gives the number of objects, and averaged coordinates of all windows in each group give the estimates of center of the objects they represent.

3.4 Frequency Diversity

Frequency diversity is often used in detection applications for two important reasons: to increase the resolution (high frequencies) and to allow radar signals to penetrate deeper into the medium (low frequencies). Therefore, with a wide frequency range, one can ideally get more resolution in the vicinity of the radar, and more penetration to probe deeper objects. To take advantage of these benefits, we use the sub-array processing in a multi-frequency scheme. For each frequency the sub-array processing described in Section 3.1 is carried out to obtain the DOAs and the crossing pattern. Then, these multiple crossing patterns are overlaid to give an aggregate crossing pattern which is modeled as Poisson counting processes in Section 3.2.

4 Examples

In this section, we present applications of sub-array processing to the detection of multiple mine-like and multiple drum-like objects. In order to simplify the scattering phenomenon associated with the detection problem, both mine-like and drum-like objects are modeled with simple, circular objects. The system parameters for both applications are kept constant to provide a better comparison of the method between applications. In order to introduce frequency diversity, the objects are illuminated with plane waves at three different frequencies: 1.2, 1.0 and 0.8 GHz. The frequency range used is typical of that used in practical subsurface sensing systems. The scattered field is observed along a 33-element, uniform, linear receiver array which spans an aperture of 1.5 m. The sensors are assumed to be ideal, isotropic receivers, and the inter-element spacing of the receivers are chosen such that it is less than half a wavelength for the soil characteristics [16] at the frequencies used. The receiver array is divided into 11 three-element sub-arrays for the processing. The objects are placed in a lossy, homogeneous background which has the same electrical

characteristics of 5% moist San Antonio clay loam or 10% moist Puerto Rico clay loam ($\epsilon_b = 6\epsilon_0$, $\sigma_b = 5 \times 10^{-2}\ S/m$) at around 1.0 GHz [16].

For the simulations, the definition of signal to noise ratio (SNR) is not obvious. In practical problems, SNR is imposed by the nature of the system noise. However, in computer simulations we want to reference the noise power to a fixed quantity that does not change as the positions of the objects change. For this purpose SNR is referenced to the scattered field strength of a single, cylindrical, metallic object placed at the same depth as the objects, in the same lossy medium. The radius of the reference scatterer is the same as the radii of the targets. With this definition, the noise power is always proportional to the power of reference scattered field, not the power of field scattered from targets which changes as the positions of objects change.

In all examples the exact scattered field due to multiple objects embedded in a homogeneous, lossy background is calculated using the recursive T-matrix algorithm [17–20] to keep the computational requirements at reasonably low levels.

4.1 Multiple Mine-like Objects

In these examples, we placed two mine-like objects, each with 7.5 cm. diameter, 15 cm. under the receiver array. Even though the algorithm is capable of detecting more than two objects, it seems that for practical purposes no more than two mines will be placed in the array's aperture of 1.5 meters. We have not explored the performance of the processing with respect to depth assuming that mine-like objects will be placed at uniform depths under the array.

The first example demonstrates the utility of the sub-array processing in detecting and localizing both a metallic and a dielectric object in the same medium. For this purpose, a metallic object and a dielectric object with dielectric constant of 2.5 are placed at $(20, -15)$ cm and $(80, -15)$ cm, respectively, in the homogeneous background described before, Fig 6. Signal to noise ratio is fixed

at 10 decibels. Fig 6 shows the directions of arrivals, and detection windows when probability of false alarm is 10^{-8}, which corresponds to a crossing threshold of $K = 7$. The two circles in this figure denote the objects, and the intertwined squares, due to overlaps in test windows, depict the estimated target windows. The detection windows are then used in the grouping algorithm described in Section 3.3. As expected two distinct groups of overlapping windows indicated that there are two objects beneath the array. The estimated center for the objects are found to be $(19.52, -14.02)$ cm and $(80.10, -14.82)$ cm. Consequently, both metallic and dielectric objects are detected within acceptable estimation error margins.

Next, we consider an example that demonstrates the detectability of objects and the performance of SAP as relative positions of the objects change. In this example, both objects are assumed to be metallic in order to see the influence of relative distance between same type of objects on detectability and estimation error. For this purpose, we fixed the location of the first object at $(x, y) = (-40, -15)$ cm. The other one is moved from $x = 0$ cm to $x = 125$ cm in the lateral direction while its depth is kept at the same level as the fixed object, Fig. 7. The signal to noise ratio is assumed to be 30 decibels.

With this geometry, the moving object is always located under the array, and thus detected for all combinations of relative positions. Detection of the fixed object, on the other hand, is challenging since it lies outside the span of the array. Fig 8 shows the average simulated probability of detection of the fixed object over 100 Monte-Carlo simulations as the other object is moved under the array when probability of false alarm is set to 10^{-3}. As it is clear from this figure, the fixed object can be detected only if the other object is well away from it. The fixed object may also be detected with less than 10% probability when the moving object is located between $x = 0$ and $x = 20$ cm. This is due to the fact that for these relative locations, both objects are close enough so

that DOAs belonging to the moving object create crossings around the fixed object as well as the moving object. In fact, because of this effect, the region between the two objects is incorrectly detected as targets, and thus false alarm rate is large when relative distance between two objects is small, Fig. 9. Simulated $P_{fa,sim}$ as depicted in Fig. 9 approaches to the false alarm rate set at the beginning of the simulation (dashed line), as the relative distance between the objects increase.

We have also investigated the effect of relative distance on estimated object centers. For this purpose, we plotted the averaged estimation error in x-direction ($\Delta x = x_{true} - x_{estimated}$) versus the averaged estimation error in y-direction ($\Delta y = y_{true} - y_{estimated}$) for both fixed and moving objects in Fig. 10(a-b). The estimated object coordinates are obtained by averaging 100 Monte-Carlo simulations. The dashed circles indicate the boundaries of the objects. The closer the symbols ($\circ$'s or $\diamond$'s) are to the center, the smaller is the estimation error. Since the moving object is always detected, each small circle in Fig. 10(a) corresponds to a different position of the moving object. As seen from this plot, the estimation error of the moving object is only a small fraction of the radius. Small circles outside the object boundary (dashed circle) correspond to locations where the moving object is close to the fixed object. Each small circle and diamond in Fig. 10(b) corresponds to a relative position when the fixed object is detected. The small circles denote the error in estimated centers when the moving object's x-coordinate is greater than 95 cm, and small diamonds correspond to other locations of the moving object for which the fixed object is detected. The loci of small circles and diamonds clearly imply that as the relative distance between the objects gets larger, the estimation error in the position of the fixed object gets smaller.

4.2 Multiple Drum-like Objects

In this section, two drum-like objects, each with 50 cm. diameter, are placed at various depths from the receiver array. Since drums are made up of metals, the objects are assumed to have

infinitely large conductivity. The signal to noise ratio is set at 10 decibels. The detection windows for a typical case is shown in Fig. 11. In this example one object is at $(-40, -125)$ cm and the other is at $(140, -125)$ cm, while the lossy, homogeneous background is the same as previous example. The threshold of detection corresponding to a false alarm rate of 10^{-8} is found to be $K = 6$. Fig. 11(b) depicts the detection windows obtained after hypothesis testing. These windows are then processed by the grouping algorithm of Section 3.3. As expected, there found to be two overlapping window groups which imply that there are two objects in the region of interest with centers located at $(-40.02, -111.70)$ cm and $(139.93, -108.46)$ cm.

As the second example of this section, we considered keeping one of the objects at a fixed location, and moving the other object around below the array. The first object is fixed at $(-40, -125)$ cm, and the other is moved from $x = 40$ cm to $x = 240$ cm in the lateral direction at two different depths, -125 cm and -137.5 cm, Fig. 12. The SNR is set to 30 dB. Contrary to mine-like object example, in this case the fixed object is at an advantageous location and detected with a probability of 1.0 regardless of the position of the moving object in the defined region. The moving object is hard to detect, since it is placed either outside the span of the array most of the time or deeper than the fixed object. Fig. 13 depicts the average probability of detection of the moving object over 100 Monte-Carlo simulations for two depths when probability of false alarm is set to 10^{-3}. It is clear that as the moving object is placed far from the array, it is less likely to be detected. Relative to the depth of the fixed object, if the moving object is placed deeper, it has to be nearer to the array to be detected. Simulated probability of false alarm ($P_{fa,sim}$) for this example is zero for all positions of the moving object, since both objects are relatively far apart to cause a false detection window.

We have also investigated the effect of relative distance and depth on estimated object centers.

For this purpose, we plotted the estimation error in x-direction ($\Delta x = x_{true} - x_{estimated}$) versus the estimation error in y-direction ($\Delta y = y_{true} - y_{estimated}$) for both fixed and moving objects for two depths in Fig. 14(a-b). The estimated object coordinates are obtained by averaging 100 Monte-Carlo simulations. The dashed circles indicate the boundaries of the objects. Circles shows the estimation errors when both objects are at the same depth, and diamonds show those when the moving object is a half radius deeper than the fixed object. Symbols (circle/diamond) inside the dashed circle indicate the estimation errors less than the radius of the object. In Fig. 14(a-b) it is observed that as the moving object gets far from the array, the estimation error in position of moving object increases, and that in position of fixed object becomes smaller. Placing the moving object at a deeper location increases the estimation error in its position, and slightly improves that in fixed object's position.

5 Conclusions

In this paper we present an algorithm that can detect and localize an unknown number of objects in the near field of a linear sensor array. The issues related to near-field scattering are overcome by partitioning the full array into sub-arrays so that the non-planar scattered field becomes locally planar at each sub-array. DOAs corresponding to these locally planar waves are then determined using array processing techniques. Triangulation of such DOAs results in dense and sparse regions of crossings which are modeled with a pair of spatial Poisson distributions. Estimated object locations, and the number of objects are finally obtained by applying a hypothesis test to Poisson models and then extracting groups of spatially disjoint detection windows.

We demonstrate the performance of the algorithm using simulated data. The usefulness of this algorithm is exhibited for both mine-like and drum-like objects. For mine-like targets, we show that

the algorithm can detect and localize multiple targets with different electrical properties. Then, we demonstrate the detectability of such objects when relative distance between them changes. We conclude that the detectability improves as the objects are located farther from each other while staying within a reasonable distance from the array. In addition, it is shown that theoretical and simulated probabilities of false alarm and detection are in agreement. For drum-like targets, we demonstrate the usefulness of the algorithm for detection and localization of multiple objects. Furthermore, the effect of relative distance and relative depth on detectability is treated. Results of this analysis supports the results obtained for mine-like objects.

As the future work, we want to combine the algorithm of this paper with the matched field processing (MFP) adapted for near-field object detection in [14]. The MFP is known for its accuracy and when used in tandem with the SAP, where SAP supplies rough estimates of object positions to MFP, it would be possible to localize closely located objects. The combined algorithm would inherit the best merits of both algorithms, viz. speed and efficiency of SAP and accuracy of MFP.

References

[1] J.W. Choi and Y.H. Kim, "Spherical Beam-Forming and MUSIC Methods for the Estimation of Location and Strength of Spherical Sound Sources", *Mechanical Systems and Signal Processing*, vol. 9, no. 5, pp. 569–588, 1995.

[2] J.W. Choi and Y.H. Kim, "Estimation of Locations and Strengths of Broadband Planar and Spherical Noise Sources Using Coherent Signal Subspace", *Journal of Acoustical Society of America*, vol. 98, no. 4, pp. 2082–2093, October 1995.

[3] Y.D. Huang and M. Barkat, "Near-Field Multiple Source Localization by Passive Sensor Array", *IEEE Transactions on Antennas and Propagation*, vol. 39, no. 7, pp. 968–974, July 1991.

[4] E.L. Miller and A.S. Willsky, "A Multiscale, Statistically Based Inversion Scheme for Linearized Inverse Scattering Problems", *IEEE Trans. on Geoscience and Remote Sensing*, vol. 34, no. 2, pp. 346–357, March 1996.

[5] E.L. Miller and A.S. Willsky, "Multiscale, Statistical Anomaly Detection Analysis and Algorithms for Linearized Inverse Scattering Problems", *Multidimensional Systems and Signal Processing*, vol. 8, pp. 151–184, 1996.

[6] A.J. Witten and J.E. Molyneux, "Ground Penetrating Radar Tomography: Algorithms and Case Studies", *IEEE Trans. Geoscience and Remote Sensing*, vol. 32, pp. 461–467, March 1994.

[7] W.C. Chew and G.P. Otto, "Microwave Imaging of Multiple Conducting Cylinders Using Local Shape Functions", *IEEE Microwave and Guided Wave Letters*, vol. 2, no. 7, pp. 284–286, July 1992.

[8] W.C Chew and Y.M. Wang, "Reconstruction of Two-Dimensional Permittivity Distribution Using the Distorted Born Iterative Method", *IEEE Trans. on Medical Imaging*, vol. 9, no. 2, pp. 218–225, June 1990.

[9] A.N. Tikhonov and V.Y. Arsenin, *Solutions to Ill-Posed Problems*, V.H. Winston & Sons, 1977.

[10] H.Krim and M.Viberg, "Sensor Array Signal Processing: Two Decades Later", Tech. Rep. CICS-P-448, Center for Intelligent Control Systems, January 1995.

[11] M. Bouvet and G. Bienvenu, Eds., *High-Resolution Methods in Underwater Acoustics*, Springer-Verlag, Heidelberg, Germany, 1991.

[12] D.L. Snyder and M.I. Miller, *Random Point Processes in Time and Space*, Springer-Verlag New York Inc., 2^{nd} edition, 1991.

[13] R.O.Schmidt, "Multiple Emitter Location and Signal Parameter Estimation", *IEEE Trans. Antennas and Propagation*, vol. AP-34, no. 3, pp. 276–280, March 1986.

[14] A. Şahin and E.L. Miller, "Object-Based Localization of Buried Objects Using High Resolution Array Processing Techniques", in *Proc. of SPIE– AeroSense:Detection and Remediation Technologies for Mines and Minelike Targets*, May 1996, vol. 2765, pp. 409–419.

[15] D. C. Hoaglin, "A Poissonnes Plot", *The American Statistician*, vol. 34, no. 3, pp. 146–149, August 1980.

[16] J.E. Hipp, "Soil Electromagnetic Parameters as Functions of Frequency, Soil Density, and Soil Moisture", *Proceedings of the IEEE*, vol. 62, no. 1, pp. 98–103, January 1974.

[17] W.C. Chew, *Waves and Fields in Inhomogeneous Media*, Van Nostrand Reinhold, 1990.

[18] L. Gürel and W.C. Chew, "A Recursive T-matrix Algorithm for Strips and Patches", *Radio Science*, vol. 27, pp. 387–401, May-June 1992.

[19] A. Şahin and E.L. Miller, "Recursive T-matrix Methods for Scattering from Multiple Dielectric and Metallic Objects", *IEEE Trans. on Antennas and Propagation*, to appear in May 1998.

[20] A. Şahin and E.L. Miller, "Recursive T-matrix Algorithm for Multiple Metallic Cylinders", *Microwave Opt. Tech. Lett.*, vol. 15, no. 6, pp. 360–363, August 1997.

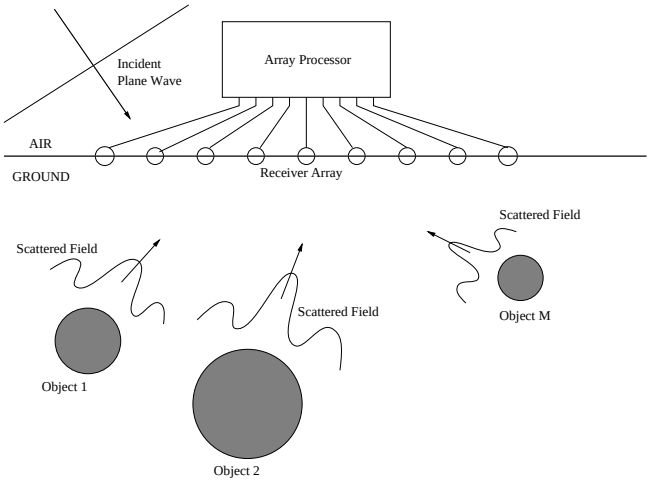

Figure 1: Problem geometry

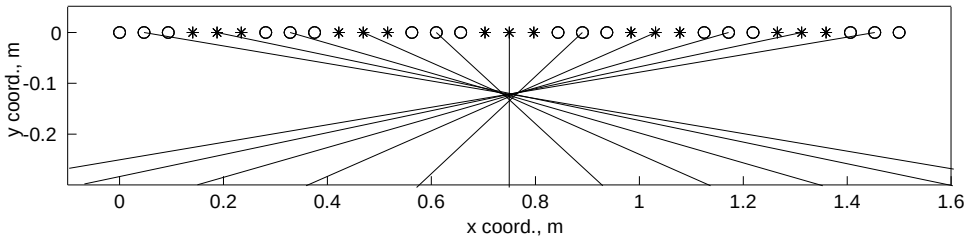

(a) DOA triangulation

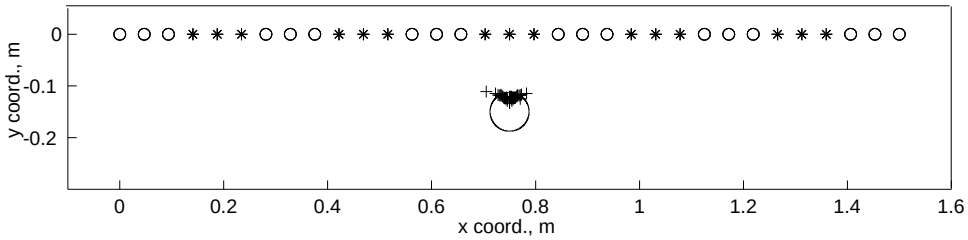

(b) Crossing pattern (+) and the object (dashed)

Figure 2: Single object localization with SAP: metallic mine-like object in lossy background

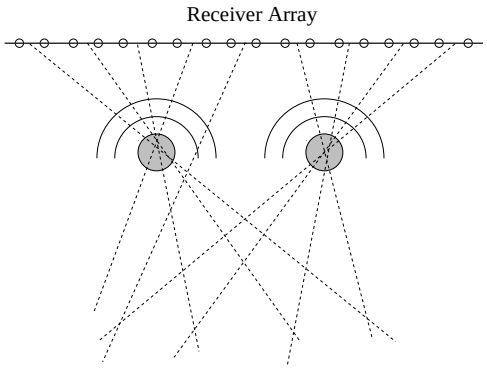

(a) Each sub-array finds one DOA

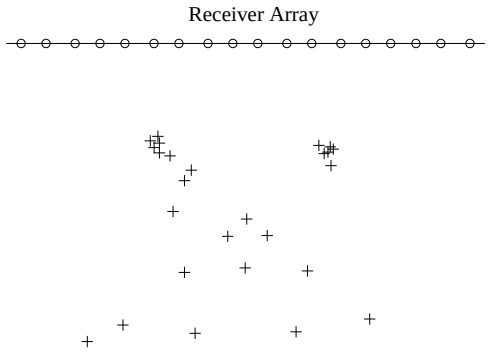

(b) Crossing pattern corresponding to DOAs in (a)

Figure 3: Multiple object subarray processing concept: directions of arrivals and crossing pattern

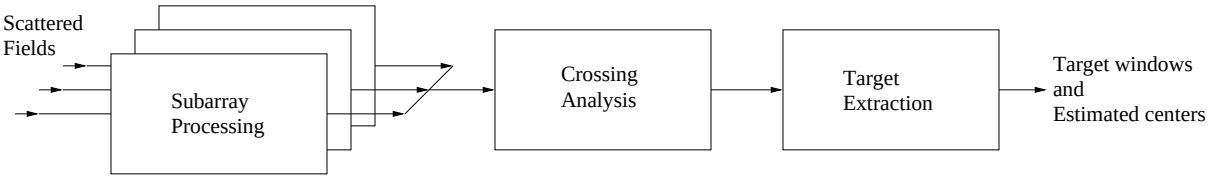

Figure 4: Flow chart of the algorithm

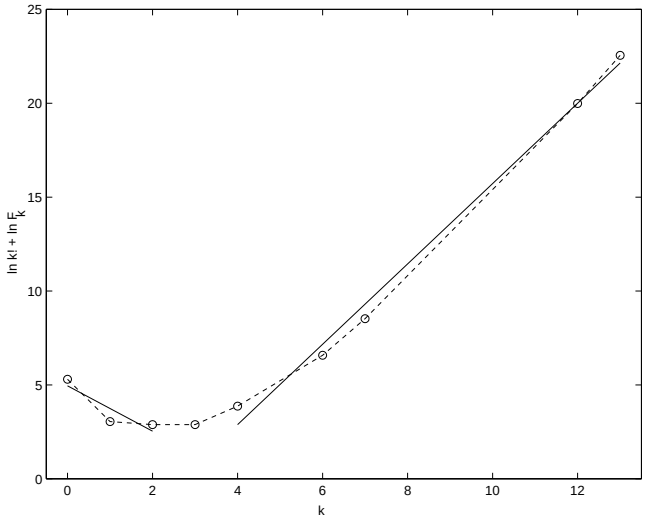

Figure 5: Fitness to Poisson model for the example of Fig. 6. Solid lines are fitted to data using linear least squares

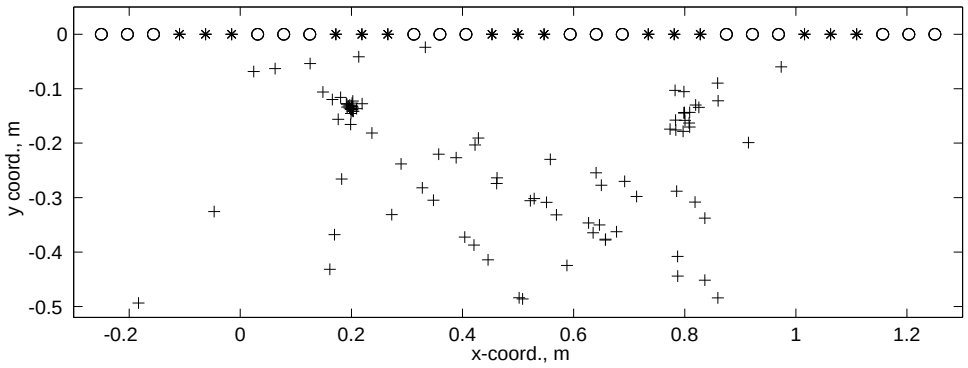

(a) DOA crossings

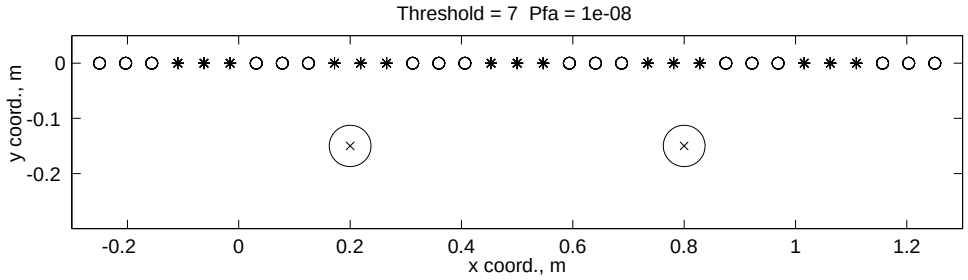

(b) Detection windows overlaid on true object positions

Figure 6: Multiple mine-like object detection with SAP: object on the left is metallic and object on the right is dielectric with $\epsilon_r = 2.5$. o's and $*$'s denote subarrays

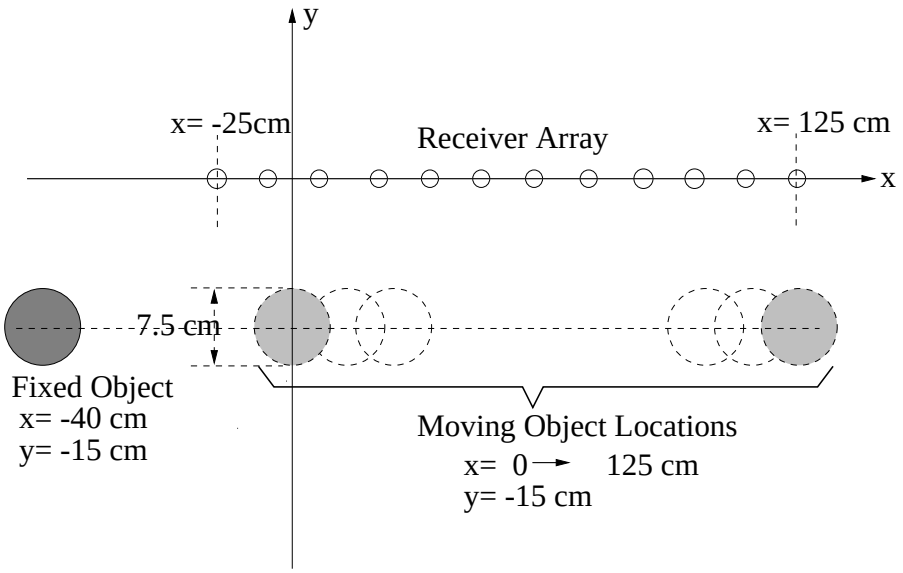

Figure 7: Multiple mine-like object detection with SAP: geometry for the example about the effect of relative distance between objects. Both objects are perfect conductors

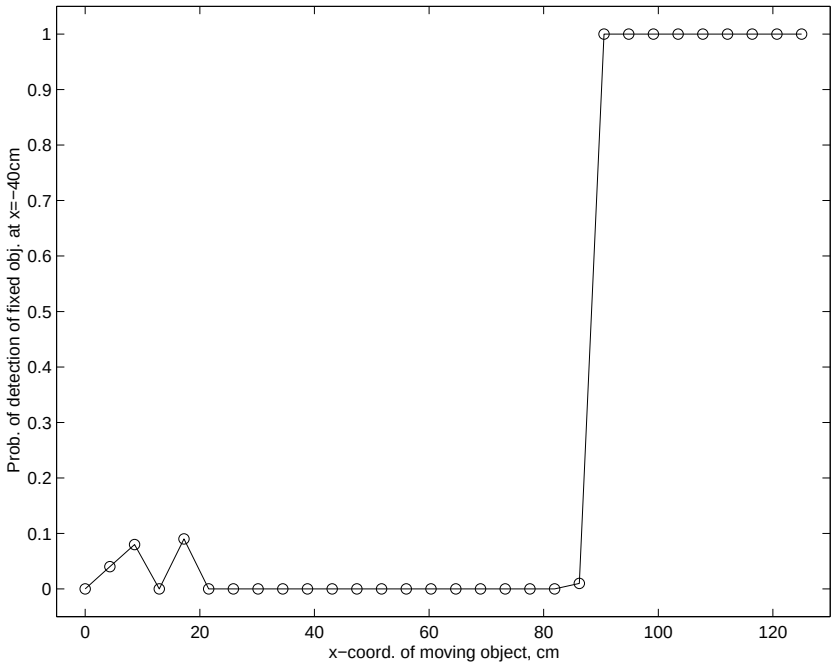

Figure 8: Probability of detection of the fixed object when the other object moves under the receiver array

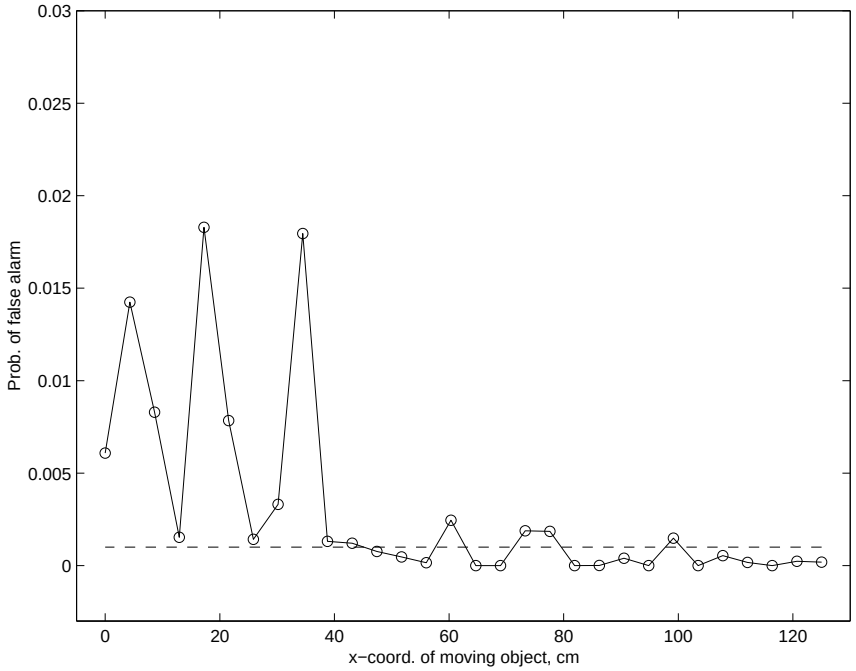

Figure 9: Probability of false alarm, when the moving object is located under the receiver array at various positions, dashed line shows the desired false alarm rate of 10^{-3}

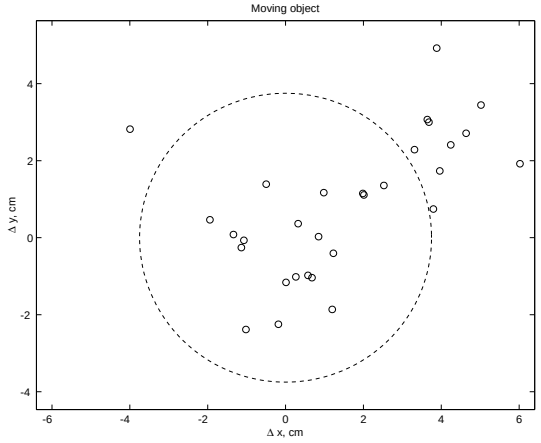

(a) Fixed Object

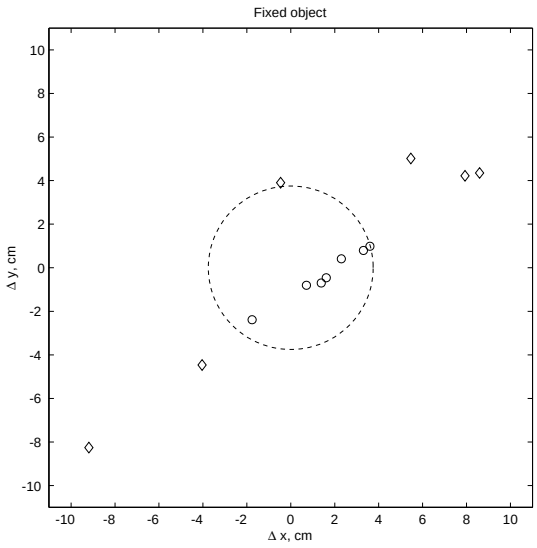

(b) Moving Object: ○'s when objects are far apart, ◇'s when they are closer

Figure 10: Estimation errors in object centers, each symbol corresponds to a different position of the moving object. Number of symbols in (b) is considerably less, since the fixed object is not detected for all positions of the moving object, see Fig. 8.

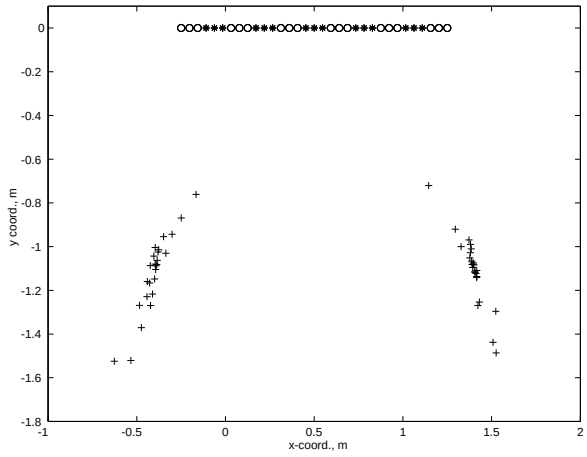

(a) DOA crossings

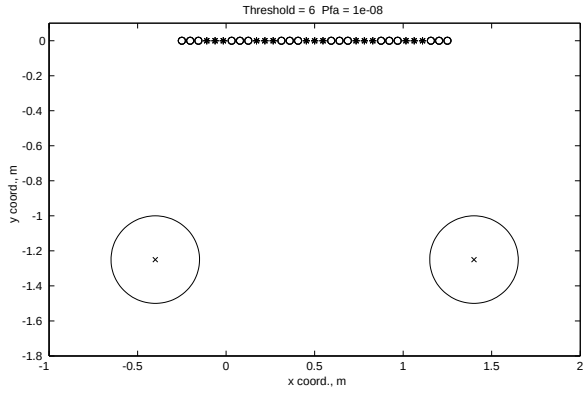

(b) Detection windows overlaid on true object positions

Figure 11: Localization of two metallic drum-like objects with SAP, ∘'s and ∗'s denote subarrays

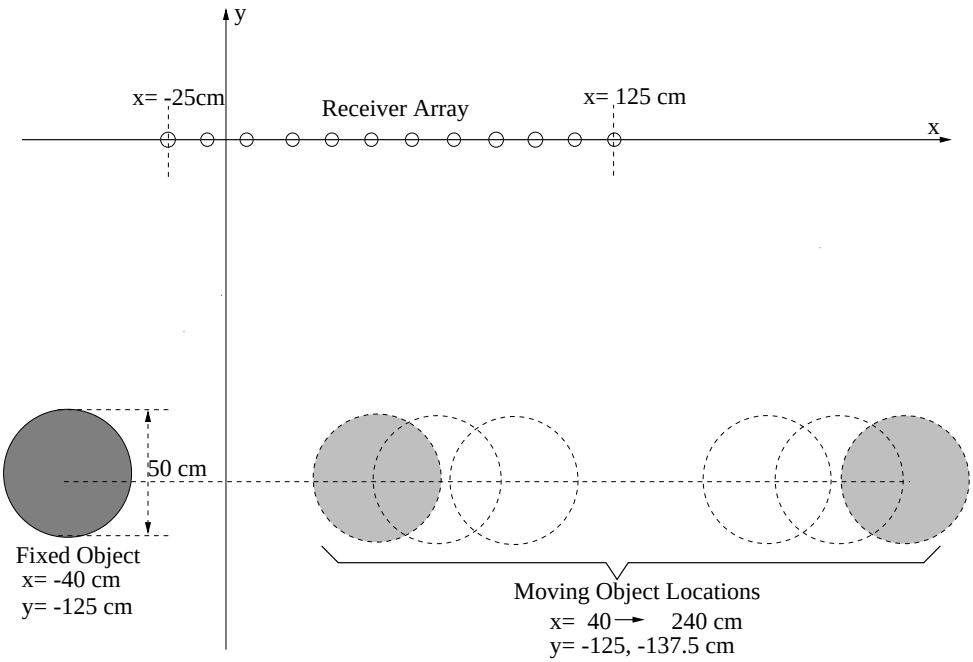

Figure 12: Multiple drum-like object detection with SAP: geometry for the example about the effect of relative distance and depth between objects. Both objects are perfect conductors

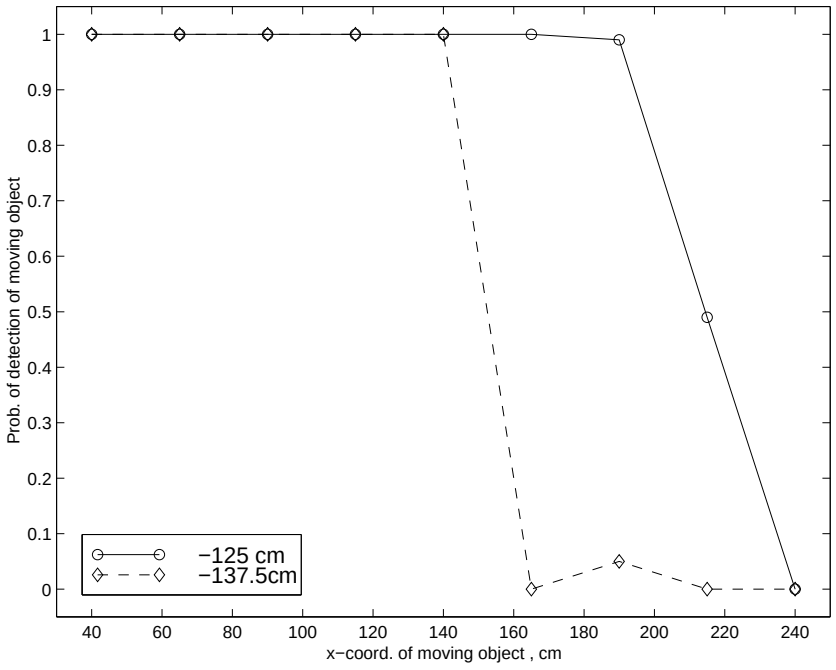

Figure 13: Probability of detection of the moving object, when the fixed object is located at (-40,-125)cm. The solid line and dashed lines show the probability of detection when the moving object is at depth -125 cm and -137.5 cm, respectively.

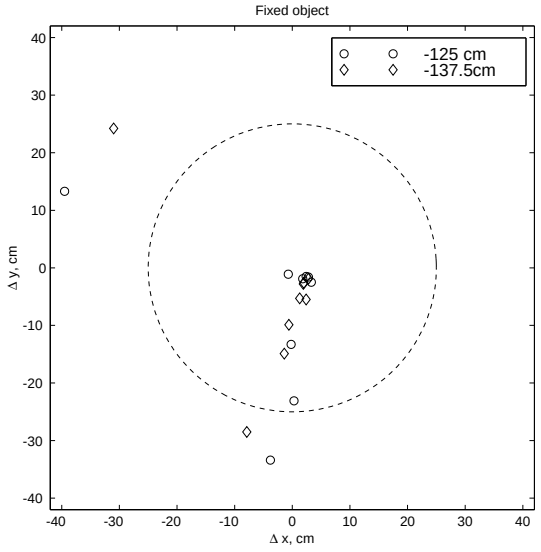

(a) Fixed Object. Depth of the moving object: o=-125 cm and ◇=-137.5 cm.

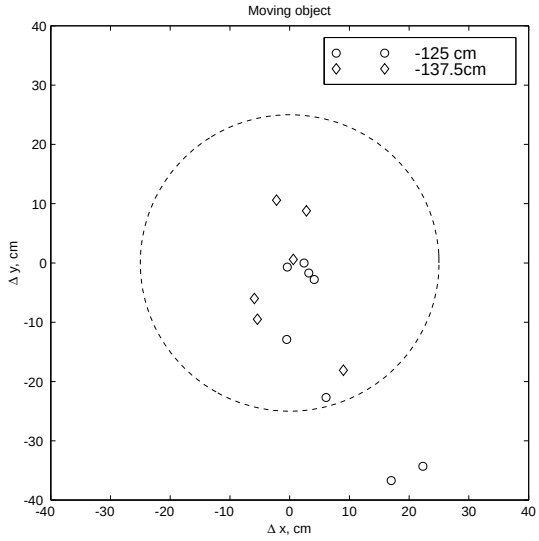

(b) Moving Object. Depth of the moving object: o=-125 cm and ◇=-137.5 cm.

Figure 14: Estimation errors in object centers, each symbol corresponds to a different position of the moving object. Number of symbols in (b) is less than that in (a), since it is not detected for all positions of the moving object, see Fig. 13.